Nanoscale Chemical Patterns on Gold Microplates

By: Cheetar Lee, Eric A. Josephs, Jingru Shao, and Tao Ye

Lee, C., Josephs, E. A., Shao, J., Ye, T. "Nanoscale Chemical Patterns on Gold Microplates." *Journal of Physical Chemistry C,* **2012***, 116* (33), 17625–17632.
https://doi.org/10.1021/jp304306w

This document is the Accepted Manuscript version of a Published Work that appeared in final form in *Journal of Physical Chemistry C*, copyright © American Chemical Society after peer review and technical editing by the publisher. To access the final edited and published work see https://doi.org/10.1021/jp304306w.

Abstract:

To generate nanoscale biochemical patterns for fundamental biophysical studies as well as practical biosensors, there remains a need for a high quality and versatile substrate. We show that chemically synthesized gold microplates on indium tin oxide are an ideal substrate that combines several desirable characteristics, including low cost, single crystallinity, optical transparency, electrical conductivity, and ease in chemical functionalization. We have developed a convenient one-pot method that allows us to synthesize plates of desired dimensions and surface coverage directly on indium tin oxide. We have used electrochemical desorption to strip the capping agents, allowing reliable functionalization with alkanethiol self-assembled monolayers. These plates can serve as nanoscale "lab benches" that allow high-resolution scanning probe lithography, high-resolution imaging, and electrical manipulation. Two applications are demonstrated here: nanoshaved self-assembled monolayers (SAMs) on the single crystalline microplates serve as a high-resolution etching resist; AFM nanografting on the plates generates SAM patterns with tailored terminal chemical functionalities.

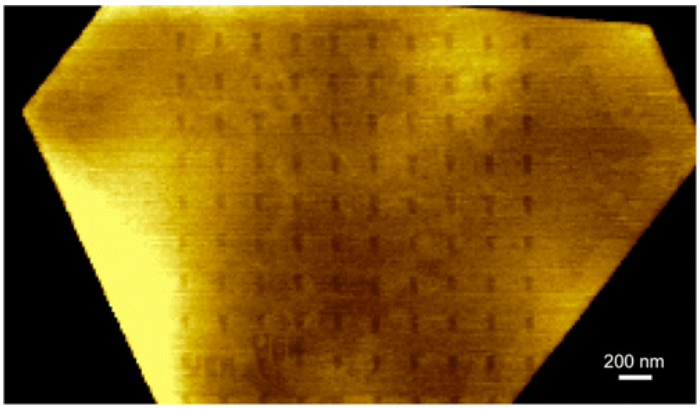

Keywords: gold microplates | self-assembled monolayers | nanografting | nanoscale chemical patterning

Article:

Gold is a ubiquitous substrate for nanoscale chemical patterns needed for sensitive arrayed biosensors[1, 2] and fundamental studies on how the nanoscale arrangement of ligands on surfaces impacts cellular processes, such as adhesion, migration, and cell fate.[3, 4] The advantages of a gold substrate include its inert chemical property, thiol–gold chemistry that allows reproducible surface functionalization with highly ordered self-assembled monolayers (SAMs),[5] electrical conductivity that enables electrical manipulation and detection,[6-8] and optical properties that allow for sensitive optical detection techniques.[9, 10] Most chemical patterns on gold are produced on continuous thin films that are deposited by evaporation or sputtering.[9, 11] Semitransparent gold thin films (10–50 nm) or nanostructures produced from such thin films are needed in many sensitive optical microscopic and spectroscopic techniques, such as surface plasmon resonance imaging, surface enhanced resonance Raman spectroscopy, and surface plasmon enhanced fluorescence.[10, 12-16] However, these thin films tend to have uncontrolled nanoscale roughness that dampens surface plasmons and produces highly variable electromagnetic field enhancement,[17, 18] hampering detection techniques that rely on the plasmonic properties of gold thin films. The surface roughness also limits the resolution of scanning probe patterning and imaging.[19] In addition, such thin film substrates, although costing significantly less than gold single crystals, remain a relatively expensive option in the biotechnology industry.[20]

We are interested in using chemically synthesized Au nano/microplates as a novel substrate for nanoscale chemical patterning to overcome the limitations associated with existing continuous films.[21, 22] Single crystalline, micrometer-sized plates can be formed by reducing Au(III) in the presence of surfactants.[23-25] These plates are terminated with atomically flat {111} facets, which have been used by Dahanayaka et al. as substrates for high-resolution scanning tunneling microscopy imaging.[22] In most existing studies, the solution-synthesized plates are purified by precipitation and resuspension before they are cast onto indium tin oxide (ITO) substrates for subsequent characterizations.[26, 27] A few studies have used a two-step nucleation and growth procedure to directly grow nanoplates on ITO,[28, 29] which eliminates the precipitation step that often causes unwanted aggregation due to strong adhesion between the plates.[27] Despite numerous studies devoted to the synthesis, structures, and optical properties of these plates,[30-32] chemical/biochemical patterning on these plates, which can impart sophisticated functions, has remained unexplored. Potential challenges in addressing the issue include convenient, reliable growth of plates of desired size, thickness, and surface coverage directly on surfaces as well as thorough removal of capping agents that impede reliable surface functionalization and patterning.

In this study, we have developed a convenient one-pot method to synthesize microplates of desired dimensions directly on ITO. We found that the capping agents used, cetyltrimethlyammonium bromide (CTAB) and iodide, can be readily removed by rinsing and reductive desorption, allowing for reproducible functionalization with alkanethiol SAMs. Both nanoshaving and nanografting[19] have been successfully performed on these micrometer-sized plates. The nanoshaved SAM could function as a high-resolution etching resist for the underlying gold, creating high-resolution metallic structures potentially useful in plasmonics. In addition, functionalized plates allow nanografting of chemical patterns with nanometer resolution. Although such plates are not yet suitable for applications that require millimeter or larger active areas, they can serve as a versatile nanoscale “lab bench” that enables high-resolution nanoscale

patterning and imaging with scanning probe techniques, electrical manipulation of the surface properties, and potentially sensitive optical measurements.[10, 12-16]

Materials and Methods

Au Microplate Growth Solution

All water used was produced by a Barnstead NANOpure Diamond analytical laboratory water purification system (18.2 MΩ·cm). In a clean 10 mL glass vial with a Teflon-lined cap, a yellow-gold translucent aqueous growth solution of 30 mM KI, 0.50 mM chloroauric acid (99.999% $HAuCl_4 \cdot 3H_2O$, Aldrich), and 20 mM cetyltrimethlyammonium bromide (99+% CTAB, Aldrich) was prepared at 70 °C. Added last to the 10 mL solution to initiate reduction was 18 μL of 0.47 M reagent grade l-ascorbic acid (Aldrich). The vial was then immediately capped and then shaken to produce a colorless solution instantaneously, after which the vial was placed in a heat bath at 70 °C.

Au Microplate/ITO (AMI) Synthesis

An ITO (Aldrich)-coated microscope slide with a surface resistivity of 70–100 Ω/sq was cut to 7 mm by 25 mm rectangular pieces and then cleaned by sonicating in acetone, ethanol, and then water for 15 min each before use. After drying the cleaned ITO under a stream of high-purity nitrogen gas, it was immersed into a freshly prepared Au microplate growth solution at 70 °C for 5 h. Once the AMI synthesis is complete, it was rinsed with acetone and then sonicated in water briefly (1–2 min) to remove the particles that were loosely bound to the surface.[22]

SAM Preparation of Au Microplates

Before forming an alkanethiol SAM on Au microplates, the electrode potential of a cleaned AMI was held at −800 mV in a 0.10 M $KClO_4$ solution for 2 min to ensure complete iodide desorption. When removing the AMI electrode from the electrolyte solution, we maintained the potential at −800 mV. The surface was then immersed into piranha solution (3:1 H_2SO_4:H_2O_2) at room temperature for 1–2 min to remove potential residual physisorbed contamination. After the surface was rinsed with water and dried under nitrogen gas, a SAM was formed on Au microplates by immersion into 1.0 mM ethanolic solutions of an alkanethiol for 24 h at room temperature. All electrochemical methods were performed with a BASi Epsilon potentiostat (Bioanalytical Systems, Inc.) using a conventional three-electrode electrolytic cell. The working electrode has an exposed area of 0.46 cm^2. A looped platinum wire was used as the counter electrode and a small Ag/AgCl 3 M KCl electrode, which has a low leakage junction, was the reference electrode. A 0.50 M KOH electrolyte was used as the supporting electrolyte. All other electrochemical methods in this paper used the same conditions presented here unless stated otherwise. UV/ozone treatment, which was explored as another iodine-stripping method, was performed with a Samco UV-1 UV ozone generator.

Sample Characterization

Au Microplates

Au microplates grown on ITO are characterized with an FEI Quanta 200 scanning electron microscope (SEM) equipped with an Everhart Thornley-SE detector and a tungsten filament as an electron source at a high voltage of 20 kV and a filament current of 2.04 A in a high-vacuum environment (10^{-6} Torr). All AFM measurements were performed with an Agilent 5500 or NT-MDT Solver-Next atomic force microscope under contact mode or tapping mode using SNL-10 (Bruker) or NS-G10 probes (NT-MDT). Because the coverage of the microplates on ITO is too low for electrochemical or IR characterization, we used evaporated Au films to model the adsorption/desorption processes on our Au microplates. Although the Au films are polycrystalline, they have a predominantly (111) texture and have been used as a convenient substrate to model single crystalline Au (111) surface in ensemble average measurements such as infrared spectroscopy.[33]

Au Films

The gold films on silicon (Platypus Technologies, LLC) were treated in freshly made piranha solution (3:1 H_2SO_4:H_2O_2) for 20 min, rinsed, and then dried under a stream of nitrogen. *Caution: piranha solution can react violently with organic materials and should be handled with personal protective equipment. Piranha solution should not be stored in tightly sealed containers.* The Au films were then lightly annealed with a hydrogen flame immediately before the surface modification procedures. SAMs formed on Au films were characterized by infrared reflection–adsorption spectroscopy (IRRAS) using a Nicolet 380 (Thermo Scientific) with p-polarized light at an incident angle of 84° from the surface normal. A gold film substrate cleaned with the piranha solution was used as the reference.

A cleaned Au film was immersed into a solution consisting of 0.10 M KI and 0.50 M KOH for 20 min for the adsorption of iodide. After rinsing the iodide-treated Au film (IAu), i.e., the working electrode, cyclic voltammetry (CV) was performed under a 0.50 M KOH electrolyte solution (IAu/KOH). As will be shown later, this electrode is compared to bare Au under other electrolyte solutions. All the voltammograms performed with Au films were acquired at a scan rate of 100 mV/s after purging with nitrogen for 20 min.

Chemical Patterning and Patterned Transfer

After an octadecanethiol SAM is formed on an Au microplate, we used AFM to selectively desorb the SAM (nanoshave) under ethanol to expose specific gold regions. The threshold of force required for AFM lithography was determined by progressively increasing the force until selective desorption was observed. Typical threshold forces applied, which depend on the sharpness of the AFM tip, range from 10 to 75 nN. Nanografting was performed under a 50 μM ethanolic solution containing the thiol to be grafted, 11-mercaptoundecanol or 11-mercaptoundecanoic acid. Pattern transfer of the nanoshaved SAM resist was achieved under an oxygen-saturated aqueous gold etchant solution containing 60 mM thiourea and 10 mM H_2SO_4. The depth changes were monitored by AFM.

Results and Discussion

Growth of Isolated, Surface Bound Au Microplates

It is advantageous to grow plates directly on surfaces to overcome the potential issue of ill-defined morphology due to aggregation of plates synthesized in solution. A few studies succeeded in synthesizing mainly nanosized plates directly on ITO using a two-step process (nucleation and growth).[28, 29] There remains need to develop a convenient one-pot method that produces a large number of 20–60 nm thick plates whose lateral dimensions are several micrometers or larger. Anisotropic gold micro/nanoplates are synthesized by reducing gold in the presence of capping agents. We chose to use CTAB and KI,[29, 34] which may be easier to remove than common polymer capping agents used, such as polyvinylpyrrolidone (PVP) and poly(ethylene glycol)[22, 28] to allow the formation of high-quality SAMs. Iodide is known to strongly adsorb on the Au (111) facets.[35-37] Working in concert with CTAB, iodide is believed to suppress the growth in [111], the direction normal to the top and bottom surfaces of a plate, while allowing for the incorporation of the gold atoms to the edges.[15, 28]

ITO substrates were directly immersed into a mixture of chloroauric acid, ascorbic acid, CTAB, and KI at an elevated temperature, 70 °C. SEM images (Figure 1A–C) showed that micrometer-sized plates were formed on ITO, and the sizes increased as the reaction time increased. To understand the role of the ITO substrate in the growth of the microplates, we immersed the substrate into an aged (4 or 9 h) growth solution for an hour. We chose the short 1 h immersion time because the growth on the surface is relatively insignificant at this time scale. Hence, the SEM images of the substrates after immersion, which only showed smaller plates at a lower surface density, reflect the morphology of the plates that were freshly deposited from the aged solutions. The absence of large plates (>20 μm) in Figure 1D,E showed that the growth of the large plates observed in Figure 1B,C predominantly occurred on the surface rather than in the solution. Even without ITO, Au microplates form a precipitate that can be collected at the bottom of the growth solution container. This provides evidence that seed particles for Au microplate growth can form in solution. We suggest a similar nucleation and growth mechanism in our one-pot method: small nanoparticle seeds formed in the solution are deposited onto ITO. These seeds then grow into larger plates on the surface. The deposition of seeds onto ITO in our one-pot growth solution can be explained by electrostatic attraction: the surfactant-capped seeds are expected to be negatively charged, and with a growth solution at a pH of 2–3, ITO (isoelectric point of about 6) is positively charged. In addition, using the glass microscope slide that has ITO deposited only on one of the two sides, we noticed that only a small number of particles formed on the glass side, and the particles were weakly bound and easily removed by sonication. We note that Au seed attachment to ITO in the presence and absence of a linker molecule, MPTMS, has been reported,[38] and the nature of the interaction that enables direct attachment of nanoparticles to ITO is not well understood.[39] Although the nucleation and growth processes in our method are combined, nucleation, which requires a high concentration of the monomer precursor, may be impeded in the later stage when gold in the solution becomes depleted.[27] Therefore, our one-pot approach is sufficient to grow plates with desired sizes. As another control, the growth solution was drop-cast onto ITO, which was then imaged with SEM (Figure S1). As expected, although there were plates formed in the solution, the plates and other structures tended to form aggregates with ill-defined morphology, in sharp contrast to the largely isolated surface grown plates observed in Figure 1. At this point, we do not know precisely why microplates grow faster on ITO than in solution. A plausible explanation is that the positive

surface charges reduce the interfacial tension and favors the growth of larger plates. A mechanistic study under way suggests that the large plates are the favored product at equilibrium. With a KI concentration of 30 mM and growth time of 5–24 h, the grown plates are 10 μm or larger in lateral size and isolated from each other. The height histogram of >200 plates measured by AFM shows that the majority of plates are between 20 and 60 nm thick (Figure 2). The thicknesses make the plates suitable for spectroscopy and microscopy techniques that exploit the surface plasmons on gold thin films.[10] We note that the parallel growth of plates was also observed in other studies that synthesized nanoplates.[28, 29] The attractive interaction between gold microplates and ITO reduces the surface energy of the plates. Plates parallel to the surface are stabilized by the attractive interactions. By contrast, plates not parallel to the surface are less stable and likely etched.

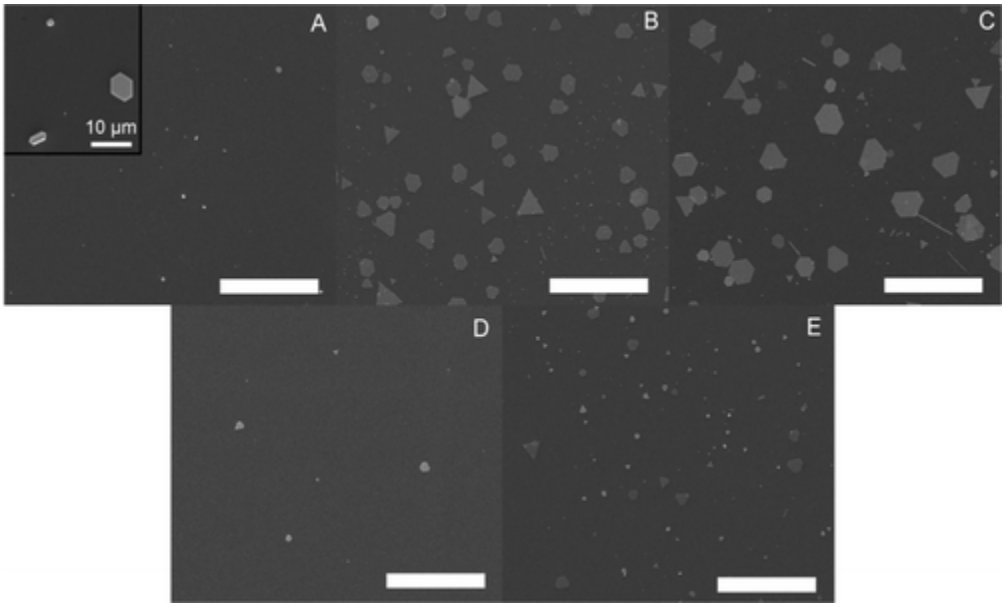

Figure 1. SEM images of Au microplates grown on ITO by immersing the substrate into a freshly prepared growth solution for (A) 1, (B) 5, and (C) 10 h. The inset of (A) shows a zoom-in image of the plates. (D) and (E) are control experiments probing the contribution of surface growth. The substrate was immersed into an aged growth solution for an hour. The solutions for (D) and (E) were aged for 4 and 9 h, respectively. All unlabeled scale bars are 100 μm.

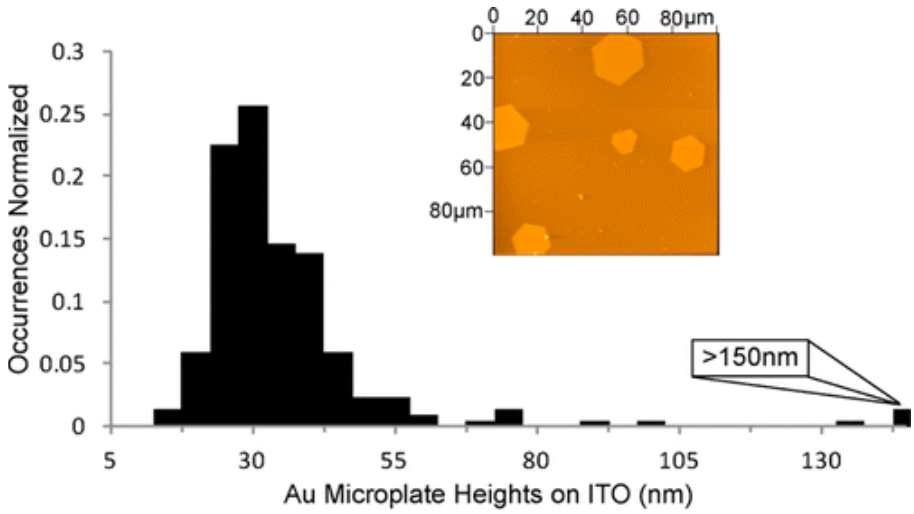

Figure 2. Au microplate thickness distribution obtained by using tapping mode AFM to scan 100 × 100 μm^2 areas (inset) on samples prepared under optimized AMI synthesis conditions.

SAM Formation on Iodine-Modified Au Substrates

Because iodide is spontaneously discharged to form zerovalent iodine when adsorbed on gold,[36] the resulting monolayer, often mentioned as iodide adlayer in other studies,[17, 34] is referred to as iodine adlayer here. While the physisorbed CTAB is readily removed by sonication in an organic solvent, the chemisorbed iodine adlayer is more difficult to remove. To investigate the potential inhibition of SAM formation by the chemisorbed iodine, an iodide-treated Au film was immersed into an octadecanethiol (ODT) solution for at least 24 h (SAM-IAu) and then compared to a typical SAM prepared on a bare Au film (SAM-Au). The cyclic voltammograms (CVs) in Figure 3B show reductive thiol desorption peaks near −1 V for both samples.[40] However, the surface coverage of ODT, Γ_{ODT}, in SAM-IAu,[36] as determined by the integrated charge of the thiol desorption peak, is only half of that for SAM-Au. In addition, the desorption peak potential of the thiol on SAM-IAu is 120 mV more positive than that for SAM-Au, suggesting that the SAM grown on iodine modified gold is more defective and less stable than an ordered SAM grown on bare gold. The CVs suggest the chemisorbed iodine partially blocks the SAM formation. Insight into partial adsorption of thiols on iodine modified gold may be gained by examining the coverage of the iodine overlayer. Electrochemical desorption has determined the surface coverage of iodine adsorbed on bare Au to be 0.274 ± 0.007 monolayer, slightly smaller than 1/3, the coverage for a ($\sqrt{3} \times \sqrt{3}R30°$) iodine overlayer on Au (111).[41] The iodine overlayer is known to be compressible, and the coverage can be increased to 0.44 under certain conditions.[41] Transient compression of the overlayer may free up a small area that allows initial adsorption of thiols to nucleate domains of SAMs. The growth of the thiol domains may lead to additional compression of the iodine adlayer and/or partial desorption of iodine. Because of the chemisorption nature, a complete desorption of the iodine adlayer may be difficult. It is worth noting that although a broad iodide desorption peak is easily identified in the CV of IAu/KOH (Figure 3A), it is not observed on an alkanethiol SAM formed on iodine modified Au film (Figure 3B and Figure S2 for LSV with an extended potential range), where iodine is expected to be present (SAM-IAu). As the adsorbed iodine atoms experience different local chemical environments and electric fields from random neighboring nanoscale SAM domains, the desorption kinetics of the iodine adlayer is expected to be highly heterogeneous. Therefore,

iodine desorption may occur over a wide range of potentials, leading to a current too small to be detectable.

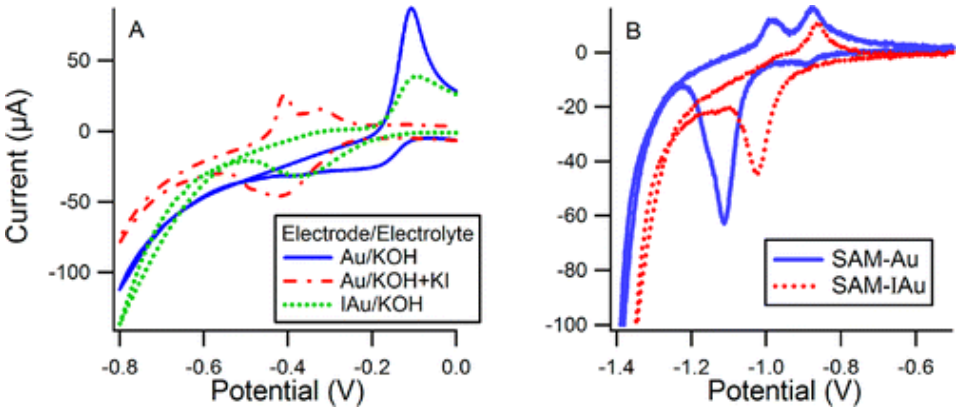

Figure 3. Cyclic voltammograms (CVs) of various modified gold film (Au) surfaces under 0.50 M KOH. Potentials are referenced against Ag/AgCl/3.0 M KCl. All CVs are scanned at 100 mV/s, under nitrogen purging, using a Pt wire as a counter electrode. (A) CV of bare Au film in 0.50 M KOH (Au/KOH), solid line, followed by an identical scan after addition of 1.0 mM KI (Au/KOH + KI), dashed line. An iodine-modified Au film under 0.50 M KOH (IAu/KOH), dotted line. (B) CV performed on a SAM of ODT on Au film (SAM-Au), solid line, and on an iodide-treated Au film (SAM-IAu), dotted line.

We also compared the grazing angle IRRAS of a SAM-Au to that of the SAM-IAu (Figure S3). The peak frequencies for various C–H asymmetric and symmetric modes are almost identical, suggesting that the degrees of molecular order in the two SAMs are similar.[33] If the ODT molecules were not uniformly adsorbed on the surface, the low coverage SAM would be more disordered and significant blue-shifts of the C–H stretch modes would be observed.[33] The IR results point to an island-like structure, where the adsorption of the ODT molecules preferentially nucleates in defects in the iodine adlayer, forming domains in which the ODT molecules are well packed, surrounded by domains of the iodine adlayer. The quantification of surface coverage using absorbance is less reliable than coulometry because it is complicated by the sensitivity to the orientation of transition dipole moment in accordance with the surface selection rule on a metal.[42] The alkyl chains in small islands may have a heterogeneous distribution of tilt angles that differ from that in a continuous SAM. Nevertheless, most of the C–H stretch absorbances are lower for SAM-IAu. For the υ_s $-CH_3$, FR mode, which is less sensitive to orientation changes, the integrated absorbance of the SAM-IAu is only about 45% of that for the SAM-Au.

AFM images of an ODT SAM formed on iodine-covered Au microplates revealed many SAM defects that are ca. 1 nm deep (Figure S4A). After we nanoshaved an area of the SAM, i.e., applied a high local pressure to desorb molecules with the AFM tip,[19] the height of the entire area was reduced to the level of the SAM defects. Therefore, the higher features correspond to patches of ODT SAM that are readily desorbed under pressure and the SAM defects correspond to the iodine adlayer. The depth of the holes is smaller than the physical thickness of an ordered ODT SAM, 2.1 nm. The difference may be attributed to the compressibility of a small SAM domain during imaging and/or higher chain tilt angles in the domain.[19] Grain analysis of the image shows that the coverage of the SAM prepared for 24 h is about 40%. Prolonged exposure

to the thiol solution, e.g., 48 h, does not increase the SAM coverage notably. The real space results obtained by AFM are consistent with the IR results, which suggest a heterogeneous surface composed of domains of the ODT SAM and iodine adlayer and that complete displacement of the chemisorbed iodine adlayer is difficult. The agreement between AFM results on the microplates and electrochemical and IR results on gold films confirms that the continuous gold film is a suitable model for the surface chemistry of these microplates, which are more difficult to characterize with many surface analysis techniques due to the low surface coverage.

The results above showed that the thiol molecules could only partially displace the chemisorbed iodine adlayer. Therefore, it is important to effectively remove the iodine adlayer for the preparation of a high-quality SAM. We first explored strong oxidants that can convert the iodine adlayer into a water-soluble, weakly adsorbed species such as iodate (Figure S4). Two methods, UV-ozone and piranha treatment, were attempted. However, the oxidant either introduced significant roughness to the gold substrate or failed to remove iodine completely.

The difficulty in forming an atomically flat gold surface by treating the surface with a strong oxidant prompted us to explore electrochemical desorption that may be minimally perturbative to gold surfaces.[36] Consistent with other studies,[36, 41] a cathodic peak at −450 mV and two anodic peaks at −400 and −350 mV were observed in the CV of a bare Au film under 1.0 mM KI and 0.50 M KOH, (Au/KOH + KI) (Figure 3A). The CV is qualitatively similar to that obtained from the Au (111) surface,[41] confirming that the Au film has a predominantly (111) texture. The electrochemically determined surface coverage of iodine, Γ_I, was $(4.56 \pm 0.75) \times 10^{14}$ atoms/cm^2. CV performed on the iodide-pretreated Au working electrode in a 0.50 M KOH electrolyte (IAu/KOH) shows a similar cathodic peak near −370 mV. The shift can be explained by the absence of KI in the electrolyte solution. The iodine surface coverage on IAu is $(3.82 \pm 0.10) \times 10^{14}$ cm^2. An anodic peak is observed near −100 mV for both IAu/KOH and bare Au in KOH (Au/KOH) CVs. However, the peak is absent for Au/KOH + KI. The anodic peak probably originated from oxidation of adsorbed impurities from the electrolyte. In the presence of a higher iodide concentration, the adsorption of impurities is blocked by the iodine adlayer on the gold surface. To test this hypothesis, we compared the CV of a bare gold working electrode under 0.50 M KOH to that under a 0.10 M $KClO_4$ electrolyte (Figure S5). Indeed, the anodic peak is not present in $KClO_4$. No further attempt was made to eliminate the impurity peak, as we found that it did not impede subsequent SAM formation.

Nanoshaving of SAM Supported on AMI Substrate

Figure 4A shows an AFM image of the alkanethiol SAM formed on the AMI substrate subjected to reductive iodine stripping. The surface morphology is consistent with a highly ordered SAM, with rms roughness of 0.11 nm. The highly ordered SAM is only possible when the chemisorbed iodine is completely removed and the flatness of the gold surface is preserved during the treatment. To demonstrate the presence of a high-quality SAM and its suitability in high-resolution chemical patterning using scanning probe lithography, we performed nanoshaving on the surface.[19] Because the micrometer sized plates are visible through the optical viewfinder of AFM (Figure S6), the tip can be positioned on specific plates for lithography. Nanoshaving on the SAM produced line widths as narrow as 30 nm (Figure 4C, top). Cross-sectional analysis over two relatively large 100 nm × 50 nm nanoshaved rectangles provides a more accurate depth

of nanoshaved pattern than thin lines (Figure 4C, bottom). The depth, 1.8 nm, is slightly smaller than the physical thickness of the ODT SAM (2.1 nm). The small difference, commonly observed in nanoshaving,[19] can be attributed to the compression of the alkyl chains by the AFM probe or a residual amount of thiol molecules adsorbed in the shaved area.

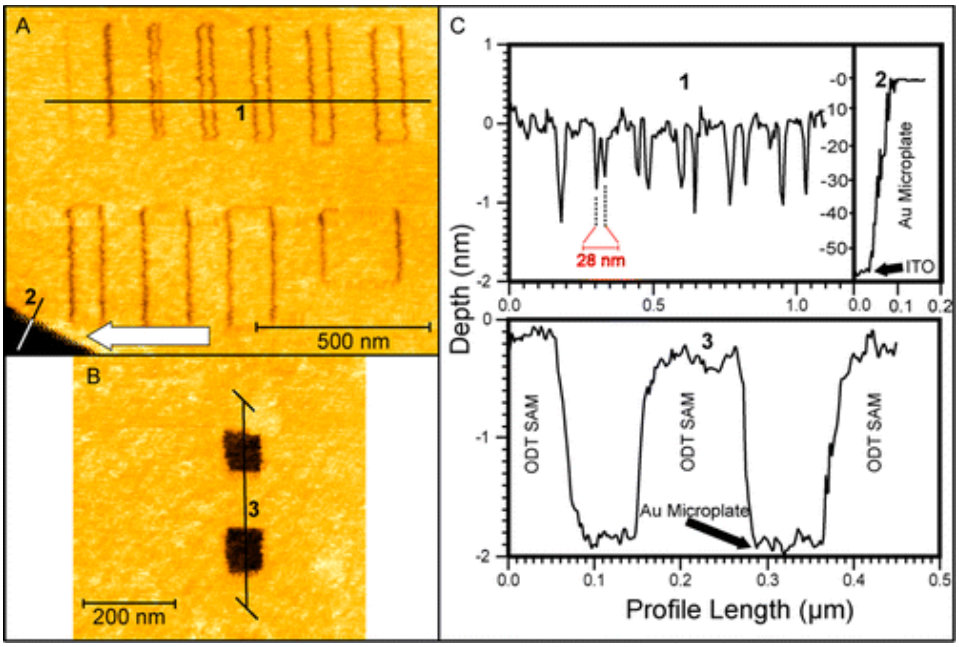

Figure 4. Contact mode AFM images of nanoshaving in ethanol of (A) filled rectangles of increasing sizes and (B) unfilled rectangles after a well-ordered densely packed ODT SAM is formed on gold microplate treated with reductive desorption. (C) Numbered height profiles corresponding to numbered lines drawn in (A) and (B). Profile 1 shows line spacings as small as 28 nm have been generated. Profile 2 shows that the plate is 60 nm thick. Profile 3 is drawn over larger nanoshaved areas to obtain more reliable thickness of the ODT SAM. White arrow in (A) indicates the microplate edge.

To further probe the quality of the SAM and demonstrate the utility of the nanoscale patterns on the AMI, we used the patterned SAM as an etching resist for the underlying gold microplate. After producing monolayer deep holes in the ODT SAM supported on a microplate, we subjected the substrate to an etching solution of thiourea saturated with atmospheric oxygen. Although in the past studies of SAM etching resists an additional oxidant such as ferric nitrate was used to oxidize gold,[43, 44] we found additional oxidants to be unnecessary as atmospheric oxygen spontaneously oxidizes gold in the presence of thiourea, consistent with a past study.[45] AFM images in Figure 5 show that after exposure to the etching solution the nanoshaved holes became deeper with only a minimal amount lateral expansion, less than 5 nm. The actual depth of the etched holes may be significantly greater than indicated by AFM, which introduces artifacts when probing high aspect ratio features due to the finite tip size.[46] For a 30 nm diameter hole, the maximum depth that can be reached by an AFM tip with a radius of curvature of 20 nm is only 13 nm. Etching is found to exclusively occur at the nanoshaved region. Figure S7 has an example showing two nanoshaved areas that are overetched; i.e., all the gold under the exposed areas had been removed, and significant sidewall etching occurred. Remarkably, even at this harsh condition, etching at areas protected by the ODT SAM was not detected by AFM. The

selective etching demonstrated in this study confirms that the SAM formed on the microplate of which the iodine adlayer had been removed electrochemically was ordered, compact, and largely impermeable to etchants. By contrast, SAMs formed on microplates which had only been treated with piranha prior to assembly could not serve as effective resists, as indicated by numerous holes formed after etching (Figure S8).

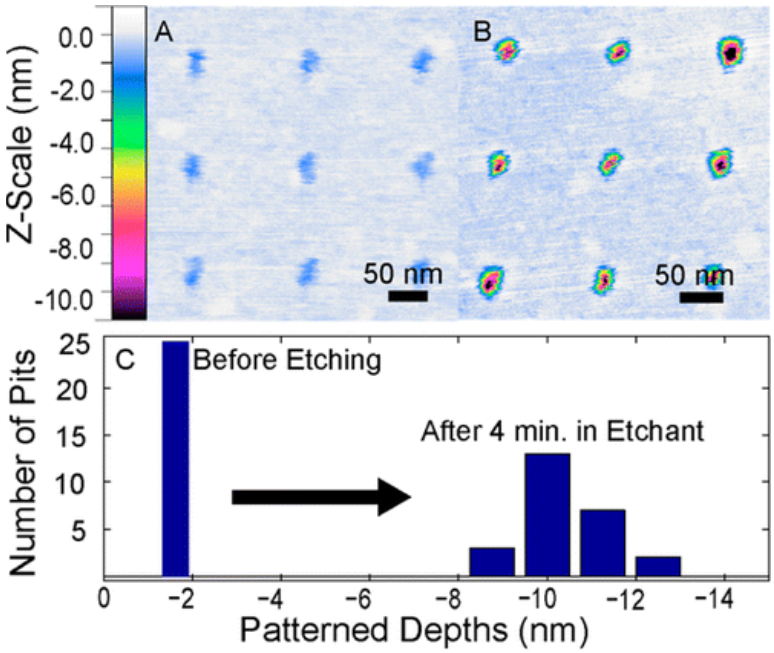

Figure 5. AFM image of patterned pits through nanoshaving of an ODT SAM on an Au microplate (A) before and (B) after exposure to an oxygenated thiourea etchant solution. (C) Histograms of pit depths.

Although patterned alkanethiol SAMs have been used as etch resists for noble metals,[47-49] they have found only limited uses in nanoscale gold plasmonic structures because they have not been competitive with electron beam lithography and FIB milling in terms of resolution and reliability.[50, 51] Our inexpensive approach may be suitable in prototyping high-resolution hole/gap structures of noble metals because nanoshaving/nanografting techniques can generate arbitrary patterns with a resolution as high as 10 nm, the highest resolution among existing SAM patterning techniques.[19] In addition, the single crystalline gold microplates may improve the resolution of pattern transfer due to the absence of nanocrytalline domains displaying heterogeneous reactivity toward etching.[31] In addition, scanning probe lithography may allow a combination of high-resolution sculpting of gold nanostructures and biochemical patterning on the nanostructure surface, which is difficult to achieve with existing EBL or FIB patterning that may be too harsh for biomolecules.[50]

Nanografting on AMI

AFM nanografting is a versatile scanning probe lithography technique that can generate chemical and biochemical patterns with a resolution as high as sub-10 nm.[19] Similar to nanoshaving, a high force is applied to the AFM tip to selectively desorb molecules in a preformed alkanethiol SAM. During nanografting, tip-induced desorption is performed in the presence of a different

thiol in the solution. The thiol molecules from the solution quickly backfill the newly exposed region, following the track of the tip. Atomically flat gold surfaces are typically used in nanografting[19, 52, 53] because they facilitate high-resolution imaging and reduce substrate-roughness-induced SAM defects[5] that can lead to deposition of new thiol molecules in unintended areas. The single crystalline microplates may be an ideal substrate for nanografting and other high-resolution scanning probe lithography techniques.[54] We performed nanografting on an ODT functionalized plate under 50 μM 11-mercaptoundecanoic acid (MUDA) and 10% v/v acetic acid in ethanol. The acetic acid was intended for suppressing the dimerization of MUDA molecules by competing for hydrogen-bonding interactions with the COOH terminal groups.[55, 56] The 75 × 90 nm^2 nanografted rectangles are about 0.7 ± 0.1 nm lower than the surrounding ODT SAM in the AFM image (Figure 6). The depth is clearly smaller than the depth of a nanoshaved area in ODT SAM (Figure 4), confirming that MUDA molecules were adsorbed. The ordered ODT SAM, with a known thickness of 2.1 nm,[57] can serve as an internal reference for measuring the thickness of the adsorbed SAM in the nanografted areas. The measured thickness, 1.4 ± 0.1 nm, is in agreement with the expected height of an adsorbed MUDA molecule in all-trans conformation with a tilt angle of 30° in an ordered SAM.[5] The thickness also suggests that bilayer formation due to the dimerization of the carboxylic acid groups[55] is minimal in the presence of acetic acid. We have also successfully nanografted 11-mercapto-1-undecanol into the ODT SAM (Figure S9). These results suggest that a minimum feature size of 20 nm can be routinely achieved on these microplates. The high resolution is typical for a highly quality SAM on a flat substrate. Additional optimizations that have been employed in nanografting on traditional gold substrates, such as optimal writing speed and direction control[53] and reversal nanografting,[58] may be used to further enhance the resolution.

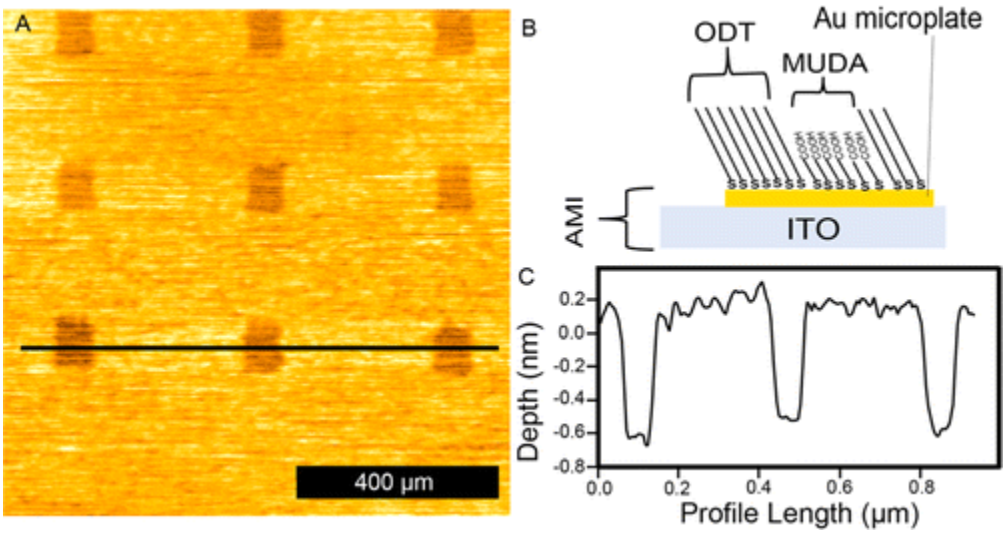

Figure 6. (A) AFM image of nanografted pattern of 11-mercapto-1-undecanoic acid in ODT SAM on an AMI substrate. (B) Side-view schematic of the proposed nanografted structure. The cross-sectional profile (C) shows that the nanografted areas are 0.7 ± 0.1 nm deep.

Conclusions

We demonstrate that isolated microplates with controlled sizes and thicknesses can be synthesized with a convenient one-pot method. We have developed reliable chemical

functionalization that is essential for nanoscale chemical patterning. Requiring only a few milligrams of gold per microscope slide, our AMI substrate is inexpensive compared to evaporated gold thin films. Although the AMI substrate is not suitable for applications requiring working areas larger than 100 μm × 100 μm, it is particularly useful for those requiring molecular scale uniformity in chemical functionalization and sub-100 nm chemical patterns.[54,59] A 10 μm × 10 μm area can easily accommodate tens of thousands features, more than sufficient for most experiments requiring nanoscale patterns. The substrate should be compatible with the single molecule nanografting technique we developed recently,[60] opening the intriguing opportunities in placing individual molecules on well-defined chemical environments on a nanoscale "benchtop" as well as manipulating and probing the molecules with single molecule techniques, such as AFM and fluorescence microscopy.[14, 61]

Supporting Information

Figures S1–S9. This material is available free of charge

Acknowledgment

We acknowledge support from UC Merced and NSF CRIF (CHE 1048651). We thank Prof Jennifer Lu's research group for technical assistance with UV-Ozone generator.

References

1. Lee, K.-B.; Park, S.-J.; Mirkin, C. A.; Smith, J. C.; Mrksich, M. Science **2002**, 295, 1702 Google Scholar
2. Sassolas, A.; Leca-Bouvier, B. D.; Blum, L. J. Chem. Rev. **2007**, 108, 109 Google Scholar
3. Chen, C. S.; Mrksich, M.; Huang, S.; Whitesides, G. M.; Ingber, D. E. Science **1997**, 276, 1425 Google Scholar
4. Hoover, D. K.; Chan, E. W. L.; Yousaf, M. N. J. Am. Chem. Soc. **2008**, 130, 3280 Google Scholar
5. Love, J. C.; Estroff, L. A.; Kriebel, J. K.; Nuzzo, R. G.; Whitesides, G. M. Chem. Rev. **2005**, 105, 1103 Google Scholar
6. Lahann, J.; Mitragotri, S.; Tran, T. N.; Kaido, H.; Sundaram, J.; Choi, I. S.; Hoffer, S.; Somorjai, G. A.; Langer, R. Science **2003**, 299, 371 Google Scholar
7. Rant, U.; Arinaga, K.; Scherer, S.; Pringsheim, E.; Fujita, S.; Yokoyama, N.; Tornow, M.; Abstreiter, G. Proc. Natl. Acad. Sci. U. S. A. **2007**, 104, 17364 Google Scholar
8. Yeo, W. S.; Yousaf, M. N.; Mrksich, M. J. Am. Chem. Soc. **2003**, 125, 14994 Google Scholar
9. DiMilla, P. A.; Folkers, J. P.; Biebuyck, H. A.; Haerter, R.; Lopez, G. P.; Whitesides, G. M. J. Am. Chem. Soc. **1994**, 116, 2225 Google Scholar
10. Lakowicz, J. R. Anal. Biochem. **2001**, 298, 1 Google Scholar

11. Wanunu, M.; Vaskevich, A.; Rubinstein, I. J. Am. Chem. Soc. **2004**, 126, 5569 Google Scholar

12. Brolo, A. G.; Arctander, E.; Gordon, R.; Leathem, B.; Kavanagh, K. L. Nano Lett. **2004**, 4, 2015 Google Scholar

13. Kang, S. H.; Shortreed, M. R.; Yeung, E. S. Anal. Chem. **2001**, 73, 1091 Google Scholar

14. Stefani, F. D.; Vasilev, K.; Bocchio, N.; Stoyanova, N.; Kreiter, M. Phys. Rev. Lett. **2005**, 94, 023005 Google Scholar

15. Vaish, A.; Liao, W.-S.; Shuster, M. J.; Hinds, J. M.; Weiss, P. S.; Andrews, A. M. Anal. Chem. **2011**, 83, 7451 Google Scholar

16. Wegner, G. J.; Lee, H. J.; Corn, R. M. Anal. Chem. **2002**, 74, 5161 Google Scholar

17. Ha, T. H.; Koo, H. J.; Chung, B. H. J. Phys. Chem. C **2007**, 111, 1123 Google Scholar

18. Kuttge, M.; Vesseur, E. J. R.; Verhoeven, J.; Lezec, H. J.; Atwater, H. A.; Polman, A. Appl. Phys. Lett. **2008**, 93, 113110 Google Scholar

19. Liu, G. Y.; Xu, S.; Qian, Y. L. Acc. Chem. Res. **2000**, 33, 457 Google Scholar

20. Müller, U. R.; Nicolau, D. V. Microarray technology and its applications. In Biological and Medical Physics, Biomedical Engineering,; Springer: Berlin, 2005; p xxii. Google Scholar

21. Base, T.; Bastl, Z.; Slouf, M.; Klementova, M.; Subrt, J.; Vetushka, A.; Ledinsky, M.; Fejfar, A.; Machacek, J.; Carr, M. J.; Londesborough, M. G. S. J. Phys. Chem. C **2008**, 112, 14446 Google Scholar

22. Dahanayaka, D. H.; Wang, J. X.; Hossain, S.; Bumm, L. A. J. Am. Chem. Soc. **2006**, 128, 6052 Google Scholar

23. Lin, G.; Lu, W.; Cui, W.; Jiang, L. Cryst. Growth Des. **2010**, 10, 1118 Google Scholar

24. Umar, A.; Oyama, M. Cryst. Growth Des. **2006**, 6, 818 Google Scholar

25. Wang, L.; Chen, X.; Zhan, J.; Chai, Y.; Yang, C.; Xu, L.; Zhuang, W.; Jing, B. J. Phys. Chem. B **2005**, 109, 3189 Google Scholar

26. Guo, Z.; Zhang, Y.; DuanMu, Y.; Xu, L.; Xie, S.; Gu, N. Colloids Surf., A **2006**, 278, 33 Google Scholar

27. Sun, X.; Dong, S.; Wang, E. Langmuir **2005**, 21, 4710 Google Scholar

28. Umar, A. A.; Oyama, M.; Salleh, M. M.; Majlis, B. Y. Cryst. Growth Des. **2009**, 9, 2835 Google Scholar

29. Zhang, D.; Diao, P.; Zhang, Q. J. Phys. Chem. C **2009**, 113, 15796 Google Scholar

30. Chu, H.-C.; Kuo, C.-H.; Huang, M. H. Inorg. Chem. **2005**, 45, 808 Google Scholar

31. Huang, J.-S.; Callegari, V.; Geisler, P.; Brüning, C.; Kern, J.; Prangsma, J. C.; Wu, X.; Feichtner, T.; Ziegler, J.; Weinmann, P.; Kamp, M.; Forchel, A.; Biagioni, P.; Sennhauser, U.; Hecht, B. Nat. Commun. **2011**, 1, 150 Google Scholar

32. Kan, C.; Zhu, X.; Wang, G. J. Phys. Chem. B **2006**, 110, 4651 Google Scholar

33. Nuzzo, R. G.; Dubois, L. H.; Allara, D. L. J. Am. Chem. Soc. **1990**, 112, 558 Google Scholar

34. Millstone, J. E.; Wei, W.; Jones, M. R.; Yoo, H.; Mirkin, C. A. Nano Lett. **2008**, 8, 2526 Google Scholar

35. Bravo, B. G.; Michelhaugh, S. L.; Soriaga, M. P.; Villegas, I.; Suggs, D. W.; Stickney, J. L. J. Phys. Chem. **1991**, 95, 5245 Google Scholar

36. Rodriguez, J. F.; Mebrahtu, T.; Soriaga, M. P. J. Electroanal. Chem. Interfacial Electrochem. **1987**, 233, 283 Google Scholar

37. Tao, N. J.; Lindsay, S. M. J. Phys. Chem. **1992**, 96, 5213 Google Scholar

38. Kambayashi, M.; Zhang, J. D.; Oyama, M. Cryst. Growth Des. **2005**, 5, 81 Google Scholar

39. Zhang, J. D.; Kambayashi, M.; Oyama, M. Electrochem. Commun. **2004**, 6, 683 Google Scholar

40. Widrig, C. A.; Chung, C.; Porter, M. D. J. Electroanal. Chem. Interfacial Electrochem. **1991**, 310, 335 Google Scholar

41. Magnussen, O. M. Chem. Rev. **2002**, 102, 679 Google Scholar

42. Sheppard, N.; Erkelens, J. Appl. Spectrosc. **1984**, 38, 471 Google Scholar

43. Weinberger, D. A.; Hong, S.; Mirkin, C. A.; Wessels, B. W.; Higgins, T. B. Adv. Mater. **2000**, 12, 1600 Google Scholar

44. Xia, Y.; Zhao, X.-M.; Kim, E.; Whitesides, G. M. Chem. Mater. **1995**, 7, 2332 Google Scholar

45. T, G. Hydrometallurgy **1976**, 1, 277 Google Scholar

46. Choi, L. S.; Kim, O. K. Langmuir **1994**, 10, 57 Google Scholar

47. Salaita, K. S.; Lee, S. W.; Ginger, D. S.; Mirkin, C. A. Nano Lett. **2006**, 6, 2493 Google Scholar

48. Wei, J. H.; Ginger, D. S. Small **2007**, 3, 2034 Google Scholar

49. Xia, Y.; Whitesides, G. M. Annu. Rev. Mater. Sci. **1998**, 28, 153 Google Scholar

50. Kinkhabwala, A.; Yu, Z.; Fan, S.; Avlasevich, Y.; Mullen, K.; Moerner, W. E. Nat. Photonics **2009**, 3, 654 Google Scholar

51. Liu, Z.; Steele, J. M.; Srituravanich, W.; Pikus, Y.; Sun, C.; Zhang, X. Nano Lett. **2005**, 5, 1726 Google Scholar

52. Zhou, D.; Sinniah, K.; Abell, C.; Rayment, T. Angew. Chem., Int. Ed. **2003**, 42, 4934 Google Scholar

53. Ngunjiri, J. N.; Kelley, A. T.; Lejeune, Z. M.; Li, J.-R.; Lewandowski, B. R.; Serem, W. K.; Daniels, S. L.; Lusker, K. L.; Garno, J. C. Scanning **2008**, 30, 123 Google Scholar

54. Lee, K. B.; Park, S. J.; Mirkin, C. A.; Smith, J. C.; Mrksich, M. Science **2002**, 295, 1702 Google Scholar

55. Kelley, A. T.; Ngunjiri, J. N.; Serem, W. K.; Lawrence, S. O.; Yu, J.-J.; Crowe, W. E.; Garno, J. C. Langmuir **2010**, 26, 3040 Google Scholar

56. Snow, A. W.; Jernigan, G. G.; Ancona, M. G. Analyst **2011**, 136, 4935 Google Scholar

57. Bain, C. D.; Troughton, E. B.; Tao, Y. T.; Evall, J.; Whitesides, G. M.; Nuzzo, R. G. J. Am. Chem. Soc. **1989**, 111, 321 Google Scholar

58. Tan, Y. H.; Liu, M.; Nolting, B.; Go, J. G.; Gervay-Hague, J.; Liu, G.-y. ACS Nano **2008**, 2, 2374 Google Scholar

59. Liu, G. Y.; Amro, N. A. Proc. Natl. Acad. Sci. U. S. A. **2002**, 99, 5165 Google Scholar

60. Josephs, E. A.; Ye, T. J. Am. Chem. Soc. **2010**, 132, 10236 Google Scholar

61. Park, H.-Y.; Li, H.-w.; Yeung, E. S.; Porter, M. D. Langmuir **2006**, 22, 4244 Google Scholar